ELSEVIER

On the extraction of neutralisation information from low energy ion scattering spectra

M. Draxler [a], J.E. Valdés [b], R. Beikler [c], P. Bauer [a,*]

[a] *Institut fuer Experimentalphysik, Johannes-Kepler Universitaet Linz, Altenbergerstrasse 69, A-4040 Linz, Austria*
[b] *Departamento de Física, Universidád Técnica Federico Santa Maria, Valparaíso, Casilla 110-V, Chile*
[c] *Max-Planck-Institut für Plasmaphysik, EURATOM Association, D-85748 Garching bei München, Germany*

Available online 22 January 2005

Abstract

There are two different ways of measuring low energy ion scattering (LEIS), i.e. detection of ions and neutrals by means of time of flight (TOF-LEIS), or detection of ions only by means of an electrostatic analyser (ESA-LEIS). We discuss, how information on charge exchange can be extracted from ESA-LEIS and TOF-LEIS spectra, respectively and which is the level of accuracy that can be expected from these procedures.
© 2004 Elsevier B.V. All rights reserved.

1. Introduction

In low energy ion scattering (LEIS), a (solid) target is bombarded with noble gas ions (He^+), the primary energy E_0 usually being in the range 1–10 keV, the angle of incidence being small (with respect to the surface normal). Ions scattered by a large angle $\theta = \pi - \alpha - \beta$ are detected, β being the exit angle (again measured with respect to the surface normal). In this regime, projectiles are scattered from surface atoms mainly by binary collisions. The use of noble gas ions (He^+) leads to sensitivity to the outermost atomic layer if only ions are detected, since noble gas ions are neutralised in the target so efficiently that projectiles backscattered from deeper layers leave the surface as neutral He atoms [1]. This is the reason, why LEIS has become a widely used surface analytical tool of quantitative composition and structure analysis [2–4].

In LEIS, the intensity of an ion peak at a certain energy [2] depends on the surface concentration of a certain species, the scattering cross section $d\sigma/d\Omega$, the ion fraction P^+ and instrumental parameters like detector solid angle and detection efficiency. A screened Coulomb potential like

---

* Corresponding author. Tel.: +43 732 2468 8516; fax: +43 732 2468 8509.
  E-mail address: peter.bauer@jku.at (P. Bauer).

M. Draxler et al. / Nucl. Instr. and Meth. in Phys. Res. B 230 (2005) 290–297

291

the Thomas–Fermi–Molière potential [5] is a reasonable basis to calculate the scattering cross section. The ion fraction P^+ is defined as the ratio A_+/A_{total}, A_+ being the yield of scattered positive ions and the denominator being the total intensity scattered into the detector. The number of detected ions A_+, i.e. the area in the ion peak, is given by

$$A_+ = \frac{N_0}{\cos \alpha} \frac{d\sigma}{d\Omega} n_s P^+ \cdot T(E_f)\Delta\Omega_+\eta_+. \tag{1}$$

Here, N_0 is the number of primary ions, n_s the number of surface atoms per area; $T(E_f)$ is the transmission probability through the analyser, which depends on the final energy of the ions E_f (after scattering), $\Delta\Omega_+$ and η_+ are the solid angle of the analyser and the detection efficiency for the ions, respectively.

A common way to measure the intensity of scattered projectiles is the use of an electrostatic analyser (ESA). In ESA-LEIS, only projectiles that leave the surface as a positive (or in principle also negative) ion can be detected. Thus, Eq. (1) is the only possibility to get access to the ion fraction P^+. It is not trivial to get absolute P^+ data from ESA spectra in this manner, since detailed knowledge on the energy dependence of T and η_+ is required.

A powerful alternative to ESA-LEIS is to use a time-of-flight (TOF) spectrometer, which analyses the velocity of the scattered projectiles by measuring the flight time along a given path (flight path). In a typical TOF-LEIS experiment, a post-acceleration voltage can be applied along the outgoing trajectory, so that ions and neutrals can be separated in a TOF-spectrum. Without post-acceleration, all charge states are detected in one spectrum. Of course, also for TOF-LEIS P^+ can be obtained from Eq. (1). In this case, at least the knowledge of T is no problem since all projectiles entering the (properly designed) flight path are transmitted. In contrast to ESA-LEIS, TOF-LEIS also yields the spectrum of scattered neutrals. Similar as in RBS, the spectrum of the neutrals also yields information from deeper layers. In TOF-LEIS, a depth resolution of better than one monolayer can be achieved by optimising the time resolution. Therefore, one can regard TOF-LEIS as a version of RBS for ultrathin layers

with a thickness range from sub-nanometers up to several nanometers, depending on experimental conditions. In analogy to RBS, the height of the neutral spectrum H_0 at the kinematic high energy limit kE_0 (with k the kinematic factor) is – within the single scattering approximation [5] – given by

$$H_0 = \frac{N_0}{\cos \alpha} \frac{d\sigma}{d\Omega} \frac{\epsilon}{[\varepsilon_e]}(1 - P^+)\eta_0\Delta\Omega_0. \tag{2}$$

Here, ϵ is the energy width of one channel, $[\varepsilon_e]$ the electronic stopping cross section factor [6,7], $\Delta\Omega_0$ and η_0 are the solid angle and the detection efficiency for the neutral He atoms, respectively. Note that Eq. (2) is a very good approximation for RBS, while its applicability is not trivial in the LEIS regime, due to strong multiple scattering in this regime (see below).

2. Charge exchange processes

Independent of the neutralisation mechanism, P^+ is related to the neutralisation probability $P^{(0)}$ via $P^+ = 1 - P^{(0)}$, applying Poissonian statistics. Since the pioneering work by Hagstrum [8], it is generally accepted that Auger neutralisation (AN) plays an important role, at least at low energies. Hagstrum derived a relation for the probability P_A^+ to survive AN in the charged state when approaching or leaving the surface. Due to the non-local character of AN, P_A^+ depends on the velocity component $v_\perp$ perpendicular to the surface ($v_\perp = \vec{v} \cdot \vec{e}$ where $\vec{e}$ is the surface normal):

$$P_A^+ = \exp\left(-\int_{-\infty}^{\infty} \frac{dt}{\tau_A(t)}\right) \approx \exp\left(-\frac{v_c}{v_\perp}\right). \tag{3}$$

This holds for in- and outgoing particles with velocities v_i and v_f, respectively. The quantity v_c has the dimension of a velocity and describes the neutralisation efficiency: It is defined as

$$v_c = \int_0^{\infty} ds[1/\tau_A(s)], \tag{4}$$

i.e. it is obtained by integration of the Auger transition rate $1/\tau_A(s)$ from 0 to ∞ over the distance s to the surface. The ion velocity v – and its parallel component $v_\parallel$ – is always small compared to the target Fermi velocity v_F. Consequently, the

effective occupation of the target states in the rest frame of the projectile is well described by the Fermi–Dirac distribution and shifted Fermi sphere effects [9] are small [10].

Apart from neutralisation along the trajectory discussed so far, charge exchange may occur also by a local process (the close collision with the backscattering centre), leading to collision induced neutralisation (CIN) and reionisation (CIR) [11]. These processes require a distance of closest approach in the collision smaller than a critical value r_{th}, therefore for a given scattering angle the associated probabilities P_{CIN} and P_{CIR} are non-vanishing only at energies E larger than a certain threshold energy E_{th}. At a given energy E, the values of P_{CIN} and P_{CIR} only depend on the impact parameter (or, equivalently, on the scattering angle θ), being independent of the scattering geometry (angles α and β).

The survival probability P^+ for the total trajectory is then obtained within the single scattering model as (see, e.g. [12])

$$P^+ = P_{in}^+ \cdot (1 - P_{CIN}) \cdot P_{out}^+ + (1 - P_{in}^+) \cdot P_{CIR} \cdot P_{out}^+, \tag{5}$$

P_{in}^+ and P_{out}^+ denote the survival probability on the ingoing and outgoing trajectory, respectively and may be calculated from Eq. (3). The two terms in Eq. (5) describe survivals and reionised projectiles, respectively. At $E < E_{th}$, $P_{CIN} = P_{CIR} = 0$ and Eq. (5) simplifies to $P^+ = P_{in}^+ \cdot P_{out}^+ = \exp[-v_c(1/v_{i\perp} + 1/v_{f\perp})] = \exp[-v_c(1/v_\perp)]$ with $1/v_\perp \equiv 1/v_{i\perp} + 1/v_{f\perp}$. Ab initio calculations of P^+ showed the importance of collision induced charge exchange processes [13,14] and experimental results obtained for He$^+$ ions and polycrystalline Cu proved the scaling properties of local and non-local neutralisation given above [15].

3. Evaluation of P^+

The conventional way to evaluate P^+ is by use of Eq. (1). For polycrystalline samples, n_s is usually taken as $n^{2/3}$, with n the atomic density of the target material. For several of the factors included in Eq. (1) the absolute values are known with a rather large uncertainty. Therefore, a usual

way to determine P^+ is to rewrite Eq. (1) in the following way:

$$\ln\left(\frac{A_+}{N_0 \frac{d\sigma}{d\Omega} E_f}\right) = \ln(P^+) + \text{const.}$$
$$= -\frac{v_c}{v_\perp} + \text{const.} \tag{6}$$

In Eq. (6) one makes use of the fact that for an ideal ESA $T(E_f) \propto E_f$ holds. Then, plotting the left hand side of Eq. (6) as a function of $1/v_\perp$, one expects a straight line in the regime $E < E_{th}$, with v_c as a slope. The unknown constant can be eliminated by extrapolating this line to 1 for $1/v_\perp \to 0$. This method has been successfully applied to study the neutralisation for many target systems [16].

For TOF-LEIS, there is an alternative way to determine P^+, i.e. by relating the peak area A_+ to the height of the neutral spectrum H_0. This method [17] is based on the fact that in an RBS spectrum H_0 is independent of multiple scattering [18]. P^+ is then obtained from

$$\frac{A_+}{H_0} = \frac{n_s[\varepsilon_e]}{\epsilon} \frac{P^+}{1 - P^+} \frac{\eta_+}{\eta_0} \frac{\Delta\Omega_+}{\Delta\Omega_0}. \tag{7}$$

Since it is very difficult to measure N_0 accurately in a TOF-LEIS experiment, it is beneficial that the ratio A_+/H_0 is independent of N_0. A further advantage of a properly designed set-up is that $\Delta\Omega_+/\Delta\Omega_0 = 1$ and only the ratio of the detection efficiencies enters. One weak point of Eq. (7) is, however, that H_0 enters, which is based on the single scattering approximation; the validity of this assumption in the present regime was shown in [19] for $0.8 < E_f/kE_0 < 1$. This may seem paradox, but can be understood on the basis that for a polycrystalline material the contribution from the outermost atomic layer is almost entirely due to single scattering with a height that is rather close to the plateau height of the spectrum (see Fig. 1).

The other weak point is that the stopping cross section ε enters, since the uncertainty of ε at these low energies is high (typically ±20% standard deviation). Nevertheless, evaluating Eq. (7) yields P^+ as

$$P^+ = \frac{1}{1 + \frac{H_0}{A_+} \frac{n_s[\varepsilon_e]}{\epsilon} \frac{\eta_+}{\eta_0} \frac{\Delta\Omega_+}{\Delta\Omega_0}}. \tag{8}$$
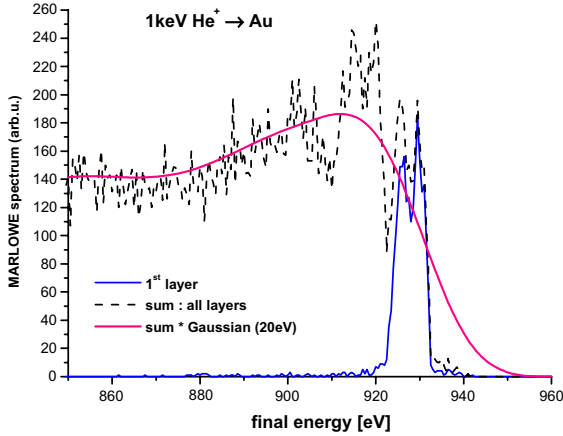
Fig. 1. Energy spectrum for 1 keV He$^+$ and polycrystalline Au for normal incidence and a scattering angle of 129°, obtained by the MARLOWE code (dashed line). The thin solid line indicates the contribution of the outermost layer (1 Å thick), the thick solid line corresponds to the MARLOWE result convoluted with a Gaussian of 20 eV width.

4. Error estimate

Obviously the quantities that enter Eqs. (6) and (8) are different. Consequently, also possible systematic errors are different. Thus, the safest way to look for possible systematic errors is to apply both procedures, as was done in [15], to obtain P^+ for He$^+$ ions and polycrystalline Cu. If by doing so concordant data are obtained from both procedures, systematic errors can be ruled out. Since it is not always possible to do so it is worth to estimate, how systematic errors in the quantities that enter Eqs. (6) and (8) will influence the resulting P^+.

In Eq. (6), the quantities that enter are N_0, $d\sigma/d\Omega$, n_s, T and η_+. Let us estimate the uncertainties of these quantities. While N_0 can be determined within 5% in an ESA experiment, it is hard to obtain the effective current in a high resolution TOF measurement with an accuracy better than 20%, since it is very low in this case. Also the absolute values of $d\sigma/d\Omega$, n_s, T and η_+ are hardly known better than ±20%, but at least for $d\sigma/d\Omega$ and η_+ the relative energy dependence (e.g. $d\sigma/d\Omega(E_1)/d\sigma/d\Omega(E_2)$) is known much more precisely. In the application of Eq. (6) it makes, however, a big difference whether a systematic

error is independent of energy and just enters the constant, or whether it depends on energy and changes the slope, as shown in Fig. 2: any change of the constant factor does not influence the ion fraction deduced, while any energy dependence of an error changes the slope and is interpreted in terms of P^+ (see Fig. 2). Consequently, it is important to know whether any error in the experimental quantities (number of primary ions, scattering cross section, number of visible surface atoms, transmission probability, detection efficiency) is constant or energy dependent.

In Fig. 2, the full straight line corresponds to Auger neutralisation (Eq. (3)) and serves as a reference line. The dashed line corresponds to the results obtained by introducing a systematic error of 65% in the constant factor in Eq. (6). In this case the resulting line is parallel to the reference line and leads to the identical slope, i.e. to the identical value of v_c. The dotted line corresponds to an energy dependent error, that is at all energies ⩽65%, but changes the deduced value of v_c by 25%. Note that these assumed errors represent a realistic upper limit of uncertainties, on the basis of 20% uncertainties attributed to the individual factors entering Eq. (6). To conclude, extreme care must be taken to arrive at a relative accuracy of ±10%

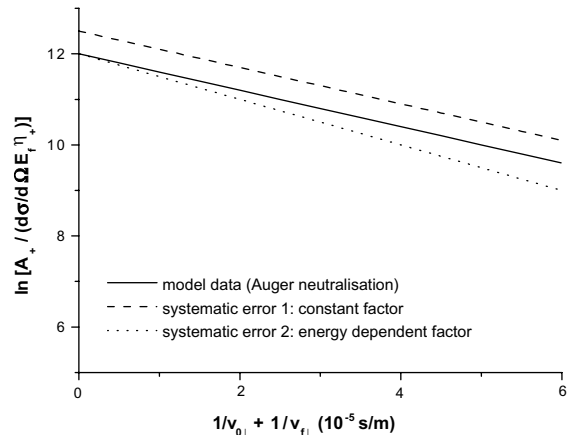
Fig. 2. Schematic representation of $\ln[A_+/(d\sigma/d\Omega E_f\eta_+)]$ as a function of the sum of inverse velocities $1/v_\perp$ (full line). The dashed line visualises the influence of a constant systematic error of 65%, the dotted line visualises the influence of a small, but energy dependent systematic error (at most is 65%), which changes the slope of the line.

or better for v_c, when deduced from Eq. (6). That this accuracy can indeed be achieved was shown by the Eindhoven group [20].

In Eq. (8), the quantities that enter are $[\varepsilon] \cdot n_s$, ϵ and the ratios η_+/η_0 and $\Delta\Omega_+/\Delta\Omega_0$. The energy width of a channel in the spectrum is obtained straightforward from experimental settings (range of the time to amplitude converter, number of channels in the spectrum, length of the flight path, masses of projectile and target atom and the primary energy), with high accuracy. Also the uncertainty of the ratio of the solid angles is very small, since in a properly designed set-up the solid angle for ions and for neutrals is identical. More problematic are the two remaining factors: (i) the energy loss in the surface layer may be calculated from $n_s = n^{2/3}$ and the stopping cross section factor. If the stopping power is assumed proportional to velocity, which is reasonable in this regime, any systematic error just enters the proportionality constant, so that the error in the factor $[\varepsilon] \cdot n_s$ is independent of energy and may be estimated from comparison of different tabulations [21,7] to be ±20%. In Fig. 3, P^+ data are shown for He$^+$ and Cu in the regime, where charge exchange is only due to Auger neutralisation. In addition to the experimental data from [22] (open symbols), also manipulated data are shown $(+, \times, *)$, which simulate the effect of an arbitrary increase in $[\varepsilon] \cdot n_s$ by 20%. The resulting data are about 15% lower and are fitted by an exponential with a v_c that is larger by 8% than the correct value. (ii) The ratio of the efficiencies is subject to a possible inherent uncertainty [23,24], since the neutrals are detected at lower energies than the ions, which are accelerated onto the micro channel plate and therefore are detected at higher energy with higher efficiency, if the first plate is operated at a negative high voltage. The corresponding uncertainty in the efficiency ratio is energy dependent. It is largest at lowest energies and may be estimated to be ±20% below 1 keV. At higher energies the detection efficiency is sufficiently large also for the neutrals and therefore the error of the efficiency ratio is small (<10% above 2 keV). The dotted line in Fig. 3 simulates a fit to data obtained by modifying the original data of [22] by an arbitrary increase of η_0 ($E_0 = 1$ keV) by 20% and of η_0 ($E_0 = 1.5$ keV) by 10%. As a result, the extrapolation to $1/v_\perp \to 0$ points to 1.45 instead of unity and the value of v_c is increased by 20% ($v_c' = 2.40 \times 10^5$ m/s).

To conclude this section, we have discussed two ways to deduce P^+ data from LEIS spectra (Eqs. (6) and (8)) and have shown how systematic errors influence the deduced ion fraction values in both cases. Care must be taken in both cases to eliminate systematic errors as far as possible and application of both approaches is beneficial in any case, due to the complementary of the quantities entering.
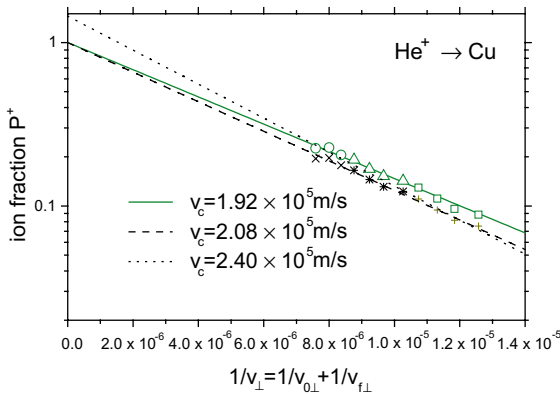

Fig. 3. Ion fraction as a function of the inverse perpendicular velocity for He$^+$ ions and polycrystalline Cu (solid line and open symbols, from [22]). The dashed line and the small symbols $(+, \times, *)$ visualise the influence of a constant systematic error of 20%, the dotted line visualises the influence of a small, but energy dependent systematic error (at most is 20%), which changes the slope of the line.

5. Determination of Auger rates

Let us discuss how Auger rates can be deduced from experimental data. As a starting point let us take a series of P^+ measurements below the threshold energy for reionisation, the results being presented in a semilog plot as a function of $1/v_\perp = 1/v_{0\perp} + 1/v_{f\perp}$ as in Fig. 2. According to Eq. (3), the experimental data should follow a straight line and extrapolate to 1 in the limit $1/v_\perp \to 0$, with a slope $-v_c/v_\perp$. So far, the evaluation of v_c does not rely on any assumption apart from the basic

scaling of Auger neutralisation with perpendicular velocity.

The conversion of v_c to the Auger rate $1/\tau_A(s)$ via Eq. (4) is, however, not straightforward, since the last part of Eq. (3) rests upon the silent underlying premise that $v_\perp$ is constant during the backscattering process and that in Eq. (4) the lower integration limit is 0. Realistically speaking, however, the minimum distance during the collision is finite (r_{min}) and the perpendicular velocity changes considerably, as is visualised in Fig. 4. In Fig. 4(a) the apex of the trajectory is shown
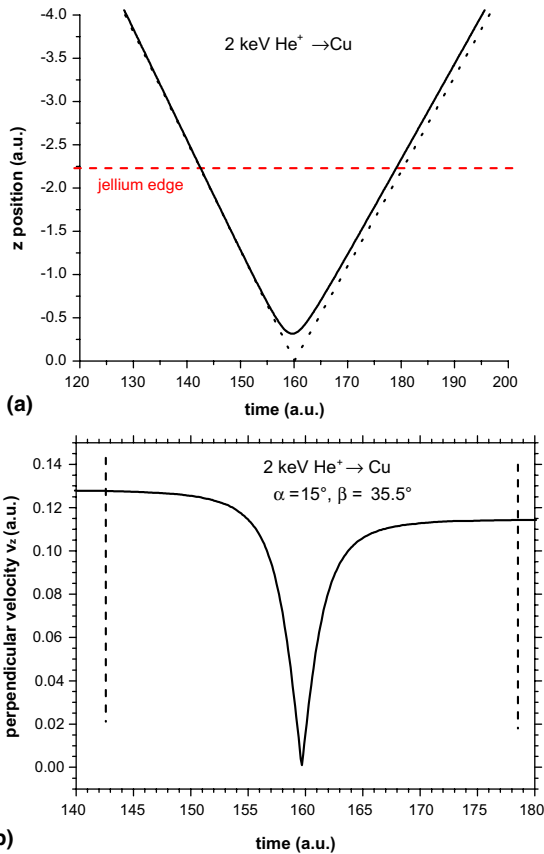

(a)

(b)

Fig. 4. (a) Trajectory of 2 keV He$^+$ projectiles scattered off a Cu(1 1 1) surface in a single scattering event ($\alpha = 25$, $\beta = 35.5°$, azimuth $\phi = 0°$). The dashed line indicates the position of the jellium edge. The dotted line corresponds to the approximative trajectory corresponding to a constant velocity on the ways in and out. (b) Vertical velocity as a function of time for scattering of 2 keV He$^+$ ions by Cu (see (a)). The vertical dotted lines correspond to passage of the jellium edge.

for 2 keV He$^+$ scattered by a Cu(1 1 1) surface in a single scattering event. The angle of incidence is 25°, the angle of exit is 35.5° and the azimuth is 0°. The minimum distance of the projectile to the surface is 0.315 a.u., i.e. 0.167 Å. Also shown is the position of the jellium edge [25]. From this, one can estimate the interaction time $\Delta\tau_n$ that is relevant for neutralisation to be 35.9 a.u. (8.67×10^{-16} s). On the other hand, for constant $v_\perp$ and $r_{min} = 0$ corresponding to straight line trajectories (see Fig. 4(a)), an approximative interaction time of 36.8 a.u. (8.89×10^{-16} s) results. Thus, to deduce a value for the Auger rate $1/\tau_A(s)$ by uncritical application of Eq. (4) would result in a systematic error of about 2.5%. To obtain more realistic information about the Auger rate, the detailed electron density in front of the surface must be taken into account. As a consequence, from $P^+(v_\perp)$ plots information about Auger neutralisation can be deduced easily. The question just is how to interpret these results: detailed information on the trajectories (z_{min}, $v_\perp (z)$) is needed to deduce realistic Auger rates from experimental raw data. Preliminary results [26] show that this systematic error can be as large as 12% in the case of 1 keV He$^+$ scattered by a Ag(1 1 0) surface.

6. Determination of local charge exchange probabilities

The preceding sections dealt with the problem how to deduce information on Auger neutralisation from experimental ion fraction data at low energies ($E < E_{th}$). Now we focus on the question, how to obtain information on local charge exchange (probabilities P_{CIN} and P_{CIR}) from P^+ measurements. For this purpose we assume that the information on Auger neutralisation has been obtained at $E < E_{th}$ and now deal with the analysis of experimental P^+ data in the regime $E > E_{th}$.

Before entering any detailed analysis, let us summarise, how P_{CIN} and P_{CIR} influence P^+. The probabilities P_{CIN} and P_{CIR} depend on E and on θ and they do not scale with $v_\perp$ as Auger neutralisation does. Consequently, there is no unique value of P^+ for a given E and a given $v_\perp$. In fact, P^+ depends strongly on the scattering

geometry, i.e. on α and β as discussed in detail in [22]. Qualitatively speaking, $\alpha \gg \beta$ corresponds to efficient neutralisation along the ingoing path and to a dominant contribution of reionised projectiles. On the other hand, $\alpha \ll \beta$ corresponds to efficient neutralisation along the outgoing path and to a small value of P^+ in any case. In other words, for a given energy a certain value of $v_\perp$ can be obtained either for $\alpha > \beta$ or for $\alpha < \beta$ with $P^+ (\alpha > \beta) > P^+(\alpha < \beta)$ Therefore, the analysis of P^+ as a function of geometry is best suited to study the influence of local charge exchange processes for a given energy.

In principle, due to local charge exchange, P^+ might appear higher or lower compared to pure Auger neutralisation ($P^+ = P^+_{in} \cdot P^+_{out}$). In general one expects $P_{CIN} > P_{CIR}$ [16] and, consequently, P^+ data below the Auger line in a semilog plot $P^+ (v_\perp)$, as has been confirmed for He ions and polycrystalline Cu target [15]. This is shown in Fig. 5(a), which presents P^+ data obtained for different values of α at a fixed primary energy, i.e. $E = 6$ keV [15]. These data exhibit the following features:

(i) The data are much lower compared to the case of pure Auger neutralisation (dashed line), due to $P_{CIN} > P_{CIR}$ (for $P_{CIN} < P_{CIR}$ the data would be above the Auger line).

(ii) The $P^+ (\alpha, \beta)$ curve has a boomerang shape with an apex at the minimum value of $1/v_\perp$. The position of this apex is close to but not identical to $\alpha = \beta$, since the projectile loses energy in the backscattering collision.

(iii) The width of this 'boomerang' is entirely due to $P_{CIR} > 0$ – for $P_{CIR} = 0$ one would obtain $P^+ = P^+_{in} \cdot (1 - P_{CIN}) \cdot P^+_{out}$, i.e. a line parallel to the Auger line (dash-dot-dotted line in Fig. 5(a)) that intersects the abscissa at $1 - P_{CIN}$ for $1/v_\perp \to 0$.

(iv) The experimental $P^+ (\alpha, \beta)$ data can be easily reproduced by Eq. (5), when P^+_{in} and P^+_{out} are known from results obtained at low energies and P_{CIN}, P_{CIR} are used as free parameters. The best fit is obtained for $P_{CIN} = 0.85$ and $P_{CIR} = 0.30$ (solid line in Fig. 5(a)). To show the influence of a variation of P_{CIR}, the dash-dotted curve has been obtained by set-

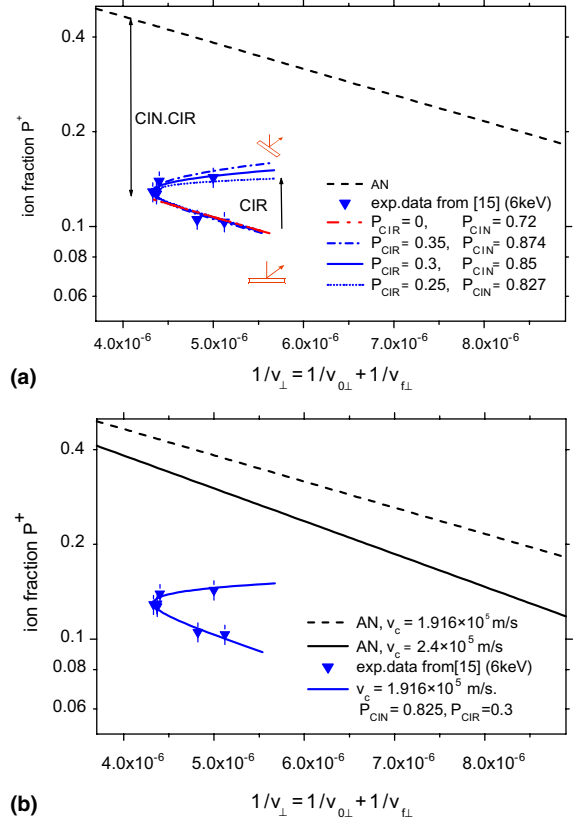

Fig. 5. (a) Ion fraction as a function of the inverse perpendicular velocity component for primary energies of He$^+$ of 6 keV for different geometries (from [15]). Making use of the value $v_c = 1.92 \times 10^5$ m/s (dashed line), the best fit to the data is obtained for $P_{CIN} = 0.85$ and $P_{CIR} = 0.3$ (solid line). Also shown are fit curves for $P_{CIR} = 0.35$ and $P_{CIN} = 0.874$ (dash-dotted line) and for $P_{CIR} = 0.25$ and $P_{CIN} = 0.874$ (dotted line). (b) The same data as shown in (a) are evaluated assuming $v_c = 2.4 \times 10^5$ m/s (bold solid line), yielding the best fit for $P_{CIN} = 0.85$ and $P_{CIR} = 0.3$ (solid line). For comparison also the original Auger line ($v_c = 1.92 \times 10^5$ m/s) is shown (dashed line).

ting $P_{CIR} = 0.35$ and by adjusting P_{CIN} to reproduce the vertical position of the boomerang, yielding $P_{CIN} = 0.874$ (dash-dotted curve in Fig. 5(a)). The dotted curve has been obtained similarly by setting $P_{CIR} = 0.25$ and $P_{CIN} = 0.874$ (dotted curve in Fig. 5(a)). Note that due to changing the P_{CIR} value the upper part of the boomerangs split up, thereby proofing the sensitivity of the boomerang width to P_{CIR}.

(v) The uncertainty of the neutralisation due to Auger processes has an influence on the values of P_{CIN} and P_{CIR} deduced from experimental data. E.g., if $v_c = 2.4 \times 10^5$ m/s is assumed for the case shown in Fig. 5, the Auger line is lower by 20% and the data are reproduced by $P_{CIN} = 0.825$ (instead of $P_{CIN} = 0.85$, see Fig. 5(b)), while P_{CIR} remains unchanged ($P_{CIR} = 0.30$). Thus, the uncertainty in P_{CIN} and P_{CIR} due to the uncertainty in v_c is small.

7. Summary

We discussed the procedures, which are commonly used to measure the fraction of ions amongst all projectiles that are scattered by surface atoms in LEIS. We presented a strategy to disentangle the contributions of local (collision induced neutralisation and reionisation) and non-local processes (Auger neutralisation) in favorable cases of sufficiently high threshold energy for the local processes. Possible sources of systematic errors in the data evaluation are discussed. To obtain a more complete understanding of the neutralisation processes also for materials with strong reionisation, further investigations are needed.

Acknowledgement

References

[1] E. Taglauer, W. Englert, W. Heiland, D.P. Jackson, Phys. Rev. Lett. 45 (1980) 740.
[2] H.H. Brongersma, P.A.C. Groenen, J.-P. Jacobs, in: J. Nowotny (Ed.), Science of Ceramic Interfaces II, Elsevier, 1994, p. 113.
[3] E. Taglauer, in: J.C. Vickerman (Ed.), Surface Analysis – The principle techniques, John Wiley Sons, 1997, p. 215.
[4] P. Bauer, in: H. Bubert, H. Jenett (Eds.), Surface and Thin Film Analysis, Wiley-VCH, Weinheim, 2002, p. 150.
[5] J.A. Leavitt, L.C. McIntyre Jr., in: J.R. Tesmer, M. Nastasi (Eds.), Handbook of Modern Ion Beam Materials Analysis, Materials Research Society, Pittsburg, 1995, p. 37.
[6] E. Rauhala, in: J.R. Tesmer, M. Nastasi (Eds.), Handbook of Modern Ion Beam Materials Analysis, Materials Research Society, Pittsburg, 1995, p. 3.
[7] J.F. Ziegler, J.P. Biersack, U. Littmark, The Stopping and Range of Ions in Solids, Vol. 1, Pergamon, New York, 1985.
[8] H.D. Hagstrum, Phys. Rev. 96 (1954) 336.
[9] J.N.M. van Wunnik, J. Los, Phys. Scrip. T 6 (1983) 27.
[10] H. Winter, Phys. Rep. 367 (2002) 387.
[11] R. Souda, M. Aono, Nucl. Instr. Meth. and B 15 (1986) 114.
[12] A.L. Boers, Surf. Sci. 63 (1977) 475.
[13] E.C. Goldberg, R. Monreal, F. Flores, H.H. Brongersma, P. Bauer, Surf. Sci. 440 (1999) L875.
[14] N.P. Wang, E.A. García, R. Monreal, F. Flores, E.C. Goldberg, H.H. Brongersma, P. Bauer, Phys. Rev. A 64 (2001) 12901/1.
[15] M. Draxler, R. Gruber, H.H. Brongersma, P. Bauer, Phys. Rev. Lett. 89 (2002) 263201.
[16] S.N. Mikhailov, R.J.M. Elfrink, J.-P. Jacobs, L.C.A. van den Oetelaar, P.J. Scanlon, H.H. Brongersma, Nucl. Instr. and Meth. B 93 (1994) 149.
[17] M. Draxler, R. Gruber, P. Bauer, J. Electron Spectrosc. Relat. Phenomen. 129 (2003) 165.
[18] Z. Smit, Phys. Rev. A 48 (1993) 2070.
[19] M. Draxler, R. Beikler, E. Taglauer, K. Schmid, R. Gruber, S. Ermolov, P. Bauer, Phys. Rev. A 68 (2003) 22901.
[20] M. De Ridder, private communication, 2004.
[21] M.J. Berger, J.S. Coursey, M.A. Zucker, ESTAR, PSTAR, and ASTAR: Computer Programs for Calculating Stopping-Power and Range Tables for Electrons, Protons, and Helium Ions (version 1.2.2). Available from <http://physics.nist.gov/Star>, 19 July 2004, National Institute of Standards and Technology, Gaithersburg, MD, 2000.
[22] M. Draxler, R. Beikler, E. Taglauer, P. Zeppenfeld, P. Bauer, Phys. Stat. Sol. (b) 241 (10) (2004) 2380.
[23] R. Cortenraad, A.W. Denier van der Gon, H.H. Brongersma, Surf. Interf. Anal. 29 (2000) 524.
[24] M. Barat, J.C. Brenot, J.A. Fayeton, Y.J. Picard, Rev. Sci. Instr. 71 (2000) 2050.
[25] P.J. Jennings, R.O. Jones, M. Weinert, Phys. Rev. B37 (1988) 6113.
[26] J. Valdez, private communication.